RSC Advances

PAPER

View Article Online
View Journal | View Issue

Cite this: *RSC Adv.*, 2024, **14**, 19483

5-step algorithm to accelerate the prediction of $[Au_{25}(SR)_{19}]^z$ clusters ($z = 1-$, 0, 1+)†

A. Tlahuice-Flores *

Received 10th May 2024
Accepted 4th June 2024

DOI: 10.1039/d4ra03458a

rsc.li/rsc-advances

Prediction of the structure of thiolated gold clusters is time demanding, and new strategies are needed to expedite this process. In this study, using one five-step algorithm and dispersion corrected density functional theory (DFT-D) calculations, new models are proposed for neutral and charged $Au_{25}(SR)_{19}$ clusters that contain one extra ligand with respect to the ubiquitous $Au_{25}(SR)_{18}$ cluster. The algorithm counts for constituting tetrahedra/octahedra units of related isomers, and it provides their energy order. In general, one structure comprising one Au_{11} inner core is found as energy minima of neutral and charged $Au_{25}(SR)_{19}$ clusters. Therefore, our new neutral structure is 0.20 eV ($-CH_3$ and TPSS) more stable than the previously reported one. With respect to neutral and anionic structures containing inner cores with C_{2v} symmetry, ultraviolet-visible/circular dichroism profiles are similar.

1 Introduction

The structural prediction of thiolated gold clusters continues due to the recent synthesis and characterization of stable clusters displaying new gold : sulphur ratios. For example, the well-known $Au_{25}(SR)_{18}^{[1-]}$ cluster comprises one Au_{13} inner core (in fact, it can be observed to contain 20 distorted tetrahedra) and 12 gold adatoms forming part of 6 staple motifs (6 dimer motifs).[1–5] Recently, Xie *et al.* reported a new size with a 25 : 19 gold : sulphur ratio found during reactions with MHA ligands (6-mercaptohexanoic acid). These ligands conferred $Au_{25}(SR)_{18}^{[1-]}$ cluster and its counterpart $Au_{25}(SR)_{19}^{[0]}$ cluster with water solubility.[6] The importance of structural isomerism and kernel atom packing is related to the selection of ligands during experiments, and some interesting properties such as photoluminescence, catalysis and optics are related to the mentioned core composition.[7–11]

Experimentally, the transformation to obtain $Au_{25}(SR)_{19}^{[0]}$ from $Au_{25}(SR)_{18}^{[1-]}$ cluster implies the introduction of one extra ligand during an oxidative etching reaction while the number of gold atoms is maintained. From a theoretical perspective, it is interesting to inquire about the induced structural change in the organic shell or inner core after introducing one extra ligand. In such a manner, the reversibility of the transformation from $Au_{25}(SR)_{19}^{[0]}$ to $Au_{25}(SR)_{18}^{[1-]}$ cluster (carbon monoxide reduction) must depend on the strength of structural distortion and energetic differences among implied species. It is important to mention that further fragmentation studies (tandem mass spectroscopy) on the produced $Au_{25}(SR)_{19}^{[0]}$ cluster revealed the presence of a lengthened motif (Au_5SR_5 unit) after ligand addition.[6] It can be interpreted as one pentameric cycle comprising the inner core of the $Au_{25}(SR)_{19}^{[0]}$ cluster.

In 2023, C. Yan *et al.* proposed a simplified structural model for a neutral $Au_{25}(SR)_{19}$ cluster (considering $-CH_3$ as a ligand) using a grand unified model (GUM).[12,13] Reported isomer comprises one low symmetry (C_1) Au_{11} core[14] and is described in terms of fused Au_3 and Au_4 blocks, while parent $Au_{25}(SR)_{18}^{[1-]}$ cluster has one high symmetry Au_{13} inner core constituting of 20 distorted tetrahedra (Au_4 units). The organic shell is also different, while the parent $Au_{25}(SR)_{18}^{[1-]}$ cluster is protected by six dimer motifs, and the $Au_{25}(SR)_{19}^{[0]}$ isomer is explained as protected by 1 pentamer, 2 trimers, 1 dimer and 1 monomer motif. However, the scarce resemblance between structural models of $Au_{25}(SR)_{18}^{[1-]}$ and $Au_{25}(SR)_{19}^{[0]}$ clusters must necessarily affect their reported reversibility of conversion.[6] The availability of $Au_{25}(SR)_{19}^{[0]}$ cluster is expected soon, but before thinking about its possible applications, it is important to study its stability under various chemical reactions. Therefore, it is important to find one proper model of the $Au_{25}(SR)_{19}^{[0]}$ cluster. Some related questions emerge: Is the Au_{13} inner core of the $Au_{25}(SR)_{18}^{[1-]}$ cluster maintained after the addition of one extra ligand? Does the $Au_{25}(SR)_{19}^{[0]}$ cluster remain stable under various charge states? For example, $Au_{25}(SR)_{18}$ cluster is very stable independent of 1−, 0, or 1+ charge-states,[15] and its stability can be explained in terms of superatom theory with an electronic counting of 8.[16] Conversely, the electronic counting of $Au_{25}(SR)_{19}^{[0]}$ cluster is 6, and to reach high stability, it may reduce (holding anionic charge-states). This manuscript addresses a major study of (neutral/charged) structures related

Universidad Autónoma de Nuevo León, CICFIM,-Facultad de Ciencias Físico-Matemáticas, San Nicolás de los Garza, Nuevo León, 66455, Mexico. E-mail: tlahuicef@gmail.com

† Electronic supplementary information (ESI) available: Detailed structures and calculated isomers by using three different ligands are provided. See DOI: https://doi.org/10.1039/d4ra03458a

to the $Au_{25}(SR)_{19}^{[0]}$ cluster, and it reports a new 5-step algorithm that can speed up their structure prediction.

2 Methodology

The DFT-D3 methodology is used during calculation as implemented in the ORCA package,[17–19] with consideration of longer-ranged van der Waals interactions using the method proposed by Grimme *et al.*[20] The generalized gradient approximation (GGA),[21] the Perdew–Burke–Ernzerhof (PBE),[22] and exchange-correlation functional were used during the full optimization stage of geometries in the gas phase. Moreover, a meta-GGA exchange-correlation functional was used during the relaxation of clusters because the Tao–Perdew–Staroverov–Scuseria (TPSS)[23] functional showed accuracy in describing aurophilic interactions in gold and related complexes, in such a manner that a better energy order among isomers is expected using it.[24,25] The def2-TZVPP Ahlrichs basis set was employed for H, S, Cl, and C atoms, and the Coulomb-fitting auxiliary basis def2/J was used. Calculations were based on the RI-J approximation. Effective core potentials were defined for Au atoms (19 valence electrons). The energy and gradient convergence criteria were selected as 1.00×10^{-6} Hartree and 3.00×10^{-5} Hartree per Bohr, respectively. This election of parameters reduced the computation time without a lack of quality in the obtained results. The obtained new structures sustaining neutral/cationic/anionic charge were fully optimized (PBE/TPSS), and their spin multiplicity corresponded with singlet or doublet. All isomers were fully structural (angles and distances graphs) and vibrationally (IR spectra) characterized.[26] Ultraviolet-Visible (UV-Vis) and circular dichroism (CD) spectra of PBE/TPSS relaxed geometries were calculated using single-point PBE calculations; TD-DFT calculations were performed by considering 300 singlet states. All depicted UV-Vis/CD spectra show a Gaussian curve with a full width at half-maximum (FWHM) of 0.1 eV.

The optimization stage of a set of candidates was performed by the initial consideration of a simple ligand, such as chloride (–Cl) and two different charge states (0, 1−). The next optimization stages were carried out by substituting chloride with –H and $-CH_3$ as ligands. The decomposition of isomers into tetrahedra/octahedra[26] is performed throughout the process to find a tendency in the energy order. This step allows us to propose new models and reduce the used time. In the final part, cationic structures were included. In this study, the discussion is dedicated exclusively to the $-CH_3$ ligand results. However, the results obtained with the –Cl and –SH ligands are provided in the ESI.†

2.1 Initial candidates

To determine the energy minimum of $Au_{25}(SR)_{19}^{[z]}$ [$z = 1-$, 0, 1+] clusters, it was considered one previously reported isomer comprising one Au_{11} inner core (C_1 point group) and protected by long staple motifs (Fig. 1a).[14]

A second isomer, including one symmetric isomer, was obtained by a slight modification of the organic shell of the parent $Au_{25}(SR)_{18}^{[1-]}$ cluster. The addition of one extra ligand turned a dimer of the $Au_{25}(SR)_{18}^{[1-]}$ cluster into one trimer motif. The insertion was done by pulling out one gold atom from the inner core toward one staple motif, leaving one Au_{12} core that preserves a central gold atom. In terms of symmetry, the parent $Au_{25}(SR)_{18}^{[1-]}$ cluster comprised one Au_{13} inner core displaying a C_i symmetry,[1] and accommodation of one gold atom from the inner core produced a pseudo-C_{2v} core (Fig. 1b). Observing a C_{2v} symmetry in the initial isomer is only possible when the trimer motif is not present and achiral ligands (such as –H or –Cl) are considered. Therefore, the symmetry of the core and gold–sulphur frameworks is reduced to the C_1 point group by the insertion of the trimer motif. The third candidate holding one Au_{13} inner core was obtained from considering a compact face centred cubic (FCC) cluster, which maintained its Au_6 and Au_4 building blocks after various optimization steps (Fig. 1c).

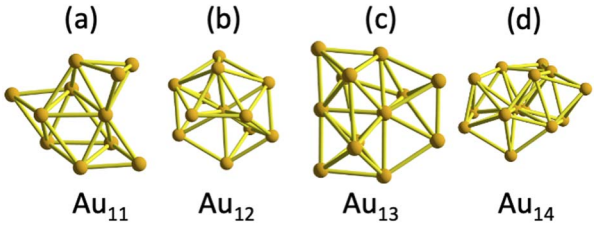

Fig. 1 The anatomy of inner cores constituting the three lowest energy isomers of $Au_{25}(SR)_{19}^{[0,1-,1+]}$ clusters under the protection of three different ligands. (a) Au_{11} core comprised 3 Au_4 building blocks, displaying a C_1 symmetry, and it corresponds with a previously published isomer,[9] (b) Au_{12} core with a loose C_{2v} symmetry, resembling a centered defective icosahedron, and it represents the new one found in this work, (c) Au_{13} core comprised by Au_4 and Au_6 units (obtained from an initial FCC cluster) and displaying C_1 symmetry. (d) Au_{14} core displaying a C_1 symmetry.

3 Results

3.1 Anatomy of calculated isomers

3.1.1 Neutral/PBE case. During the optimization stages, structural changes were observed because of changes in the ligand type; for example, the substitution of $-CH_3$ ligands in the previously relaxed cluster with –H ligands yielded one pentamer motif because of the fusion of a pair of dimer motifs. This increment in the number of gold adatoms resulted in a decrease in one gold atom in the inner core. The described anatomy agrees with experimental findings of lengthened motifs constituting the $Au_{25}(SR)_{19}^{[0]}$ cluster.[6] Energy minimum corresponds with the isomer containing one Au_{11} core with a loose C_s symmetry (Fig. 1a and previously reported[14]). Another isomer (0.14 eV relative energy or RE value) contains one Au_{11} inner core displaying a C_{2v} point group (Fig. 1b) and protected by 5 dimers and 1 trimer motif. The third isomer in energy has one Au_{13} core with a 1.05 eV RE value (Fig. 3d in ESI†). The fourth place (1.24 eV) is taken from one isomer constituted by one Au_{13} core (Fig. 1c) and protected by 5 dimer and 2 monomer motifs. For this case, the

energy minimum comprises one Au_{11} core and one octahedron and 4 compact tetrahedra.

3.1.2 Neutral/TPSS case. With the change from PBE to TPSS XC-functional, a reversed energy order is obtained. In such a manner, our new isomer constituted by one Au_{11} inner core (C_{2v}) was found as the energy minimum (Fig. 1b). The second in energy isomer (0.2 eV RE value) corresponds to an isomer whose inner core features a C_s point group and is related to the core depicted in Fig. 1a. One isomer comprising one Au_{14} core (see Fig. 1d) shows a 0.53 eV RE value. The isomer constituting of Au_{13} inner core (Fig. 1c) is found with an RE value of 0.6 eV.

3.1.3 Anionic/PBE case. The energy minimum corresponds to our isomer holding one Au_{11} (C_{2v}) inner core (Fig. 1b). With a −1 charge state, the reported isomer holding one Au_{11} inner core (Fig. 1a) is 0.42 eV separated from the energy minimum, while the isomer with Au_{13} core (Fig. 1c) displays a 1.07 eV RE value. Clearly, the introduction of charge resulted in large energy differences among isomers, and our new isomer (C_{2v}) is found as stable even after the change in its charge-state.

3.1.4 Anionic/TPSS case. As in the anionic/PBE case, the energy minimum comprises one Au_{11} inner core with a C_{2v} symmetry. The second in energy (0.43 eV) is holding one Au_{14} core (Fig. 1d), and the Au_{11} isomer displaying a 0.69 eV RE value corresponds to that previously reported by Yan *et al.* (Fig. 1a). This result can be interpreted as a strong effect in the neutral isomer holding a C_s symmetry after a change in its charge state.

3.1.5 Cationic/PBE case. Once the energy order and type of isomers were determined for neutral and anionic structures, isomers holding Au_{11} inner cores were considered for cationic clusters. The energy minimum corresponds to our new isomer containing one Au_{11} inner core (Fig. 1b). Moreover, the second one corresponds to one Au_{11} isomer (Fig. 1a) protected by 1 pentamer, 2 trimers, 1 dimer, and 1 monomer motif, displaying a 0.53 eV RE value. These results revealed a major energy separation among isomers with a clear preference for our new $Au_{25}(SR)_{19}^{[1+]}$ cluster.

Further examination of all the considered cases allows us to summarize our results as follows:

(a) Neutral isomer is constituted by one Au_{11} inner core, and it coincides with that reported previously[14] only when the PBE XC-functional was used. This isomer was found to be a minimum when –H or $–CH_3$ were considered ligands. However, the neutral charge-state and TPSS functional gave a preference for isomers holding one Au_{11} core with C_{2v} symmetry.

(b) The charge-state effect on isomers can be observed as large energy differences between them. For example, anionic structures calculated with PBE displayed a major preference for isomers comprising C_{2v} cores (by around 0.42 eV RE value); anionic charge and TPSS increased this energy preference to approximately 0.69 eV RE value. Finally, the cationic/PBE combination displayed a preference of 0.53 eV for isomers containing one Au_{11} (C_{2v}) core.

(c) When chloride was used as a ligand, energy minima corresponded with isomers comprising Au_{13}/Au_{14} cores, independent of charge state or used XC-functional (PBE or TPSS).

3.2 Polyhedra analysis of energy minima (bond length dispersion graphics)

Other structures obtained by considering –Cl and –H ligands with 0, −1, and +1 charge states are provided in the ESI.† Combinations of charge-state/$–CH_3$ gave various isomers with Au_{11} inner cores displaying close RE values. In such a manner, a natural question emerged: what variable can be used to distinguish among isomers? A response was found after a polyhedra analysis of the optimized structures with our improved FORTRAN code (available upon request).[26] This code determines the numbers of octahedra and tetrahedra that constitute protected-gold clusters and allows us to classify them in terms of their bond lengths as distorted tetrahedra or compact tetrahedra. Herein, the compact tetrahedra term refers to Au_4 units with edges included in the range of 2.6–3.2 Å (to account for distances comparable to Au (core)–Au (core) distances), while consideration of distorted tetrahedra requires bond lengths of around 3.4 Å (experimental aurophilic bonding is determined in the range of 3.02–3.27 Å from the crystal).[1]

The justification for considering tetrahedra and octahedra as part of thiolated gold clusters is that they are reduced to small pieces from bulk gold (having an FCC structure) and perturbed by sulphur atoms. In such a manner that, for thiolated gold, clusters seem viable to account for the number of tetrahedra and octahedra and the study of their edge lengths and face angles.

Their decomposition into polyhedra can be done for the full structure (inner core + gold–sulphur framework) by considering only their inner core. This analysis can reveal the number of polyhedra and the distribution of compact tetrahedra along the cluster anatomy.

Further polyhedral analysis reveals that the energy minimum of the neutral cluster (calculated with PBE XC-functional) is constituted by one octahedron and 4 compact tetrahedra (Fig. 2). However, using the TPSS XC-functional, the more stable isomer (C_{2v} symmetry) features 12 compact tetrahedra instead of an isomer containing one octahedron.

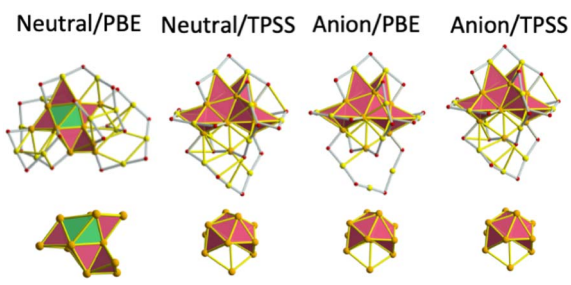

Fig. 2 Anatomy of energy minima of $–CH_3$ protected $Au_{25}(SR)_{19}^{[0,1-]}$ clusters. Tetrahedra faces are shown in red colour and octahedra in green. A combination of neutral/PBE gave energetic preference for isomer is constituted by one Au_{11} inner core. A major preference for isomers comprising one Au_{11} (sustaining a C_{2v} symmetry) inner core is obtained for other combinations of charged structures (independent of the XC-functional used). Colour code: orange stands for gold atoms in the inner core; yellow represents gold atoms in staple motifs; and red spheres represent S atoms.

In general, clusters holding a 1-charge state were found as energy minima when more tetrahedra formed part of the structure, independent of the XC-functional.

Based on the obtained results, it was determined that the stability of the isomers of $Au_{25}(SR)_{19}^{[z]}$ clusters [$z = 1-$, 0, 1+] can be related to the number/type of constituting polyhedra. Therefore, to gain insight into this correlation, the following formula was proposed:

$$\text{T-factor} = \frac{\text{Number of octahedra} + \text{Number of tetrahedra}}{\text{Number of compact tetrahedra}}.$$

A better agreement between the given formula and the energy order of the studied isomers is found in the following five steps:

(1) Find all constituting polyhedra (tetrahedra/octahedra) of the full structure (Au–S framework + inner core) and its inner core (compact tetrahedra or cT) for each isomer separately. Be aware that in full structure, Au–Au bond lengths are included in the range from 2.6 to 3.4 Å, while compact tetrahedra display bond lengths included in the range from 2.6 to 3.2 Å.

(2) Sort all isomers for each combination of the charge-state/XC-functional in descending order of constituting tetrahedra.

(3) Form sets with isomers displaying the same type of polyhedra. This means that isomers holding only tetrahedra must be included in one set, and those comprising a combination of octahedra and tetrahedra must form another set. In Fig. 3, text boxes allow us to distinguish each set of structures.

(4) Calculate the T-factor value (T-f) using the given formula. When the number of compact tetrahedra is zero, to avoid zero division, the counting of tetrahedra is repeated by increasing the Au–Au bond lengths.

(5) Look for T-factor value in each set, and make sure that if this value is small, the full set (with all its isomers) needs to shift toward the left position to maintain the ascendent order in terms of factor value.

Remarkably, after applying step number (5), it is possible that the more stable isomers do not have a large number of tetrahedra, but the major stability can be related to a large T-factor value (proportion among constituting polyhedra).

In this study, a 5-step algorithm was helpful to distinguish among isomers of the neutral $Au_{25}(SCH_3)_{19}$ cluster and to predict their expected energy order (Fig. 3). Proper schemes showing the implementation of the 5-step algorithm for each combination of the charge-state/ligand/XC functional are illustrated in Fig. S2.†

The obtained results can be summarized as follows.

(1) Chloride-protected clusters show an energy order consistent with a decrement in their calculated T-factor values. This means that the energy minimum corresponds to a large T-factor value. This result is independent of charge-state or XC-functional.

(2) Conversely, for H-protected clusters, more stable isomers correspond with small T-factor values. This rule applies to all studied charge-states/XC-functional combinations.

(3) CH_3-protected clusters display an energy order with increment in T-factor values. The energy minimum holds a smaller T-factor value. A reversed order was found only for the combination of cationic/PBE cases.

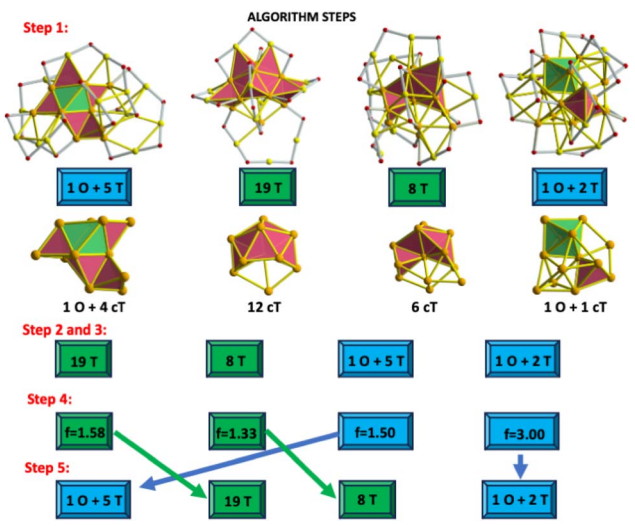

Fig. 3 Implementation of a 5-step algorithm to determine the energy order between isomers of the $Au_{25}(SCH_3)_{19}^{[0]}$ cluster. Colour code is the same as that shown in Fig. 2. Upper panel features the number and type of polyhedra found in each total structure (Au–S framework + inner core). The lower panel depicts compact tetrahedra (cT) constituting each inner core. Each step of the algorithm is given in the lower part. Highlighted boxes are used to distinguish between two sets of structures. The last row (step number 5) contains the ordered structures in terms of the corresponding T-factor values.

3.3 Optical and chiroptical properties of $Au_{25}(SCH_3)_{19}^{[1-,\ 0,\ 1+]}$ clusters)

Neutral and PBE XC-functional yielded an energy minimum containing Au_{11} inner core with C_s symmetry. Its calculated UV-Vis lineshape shows 4 peaks (Fig. 4) included in the range from 1.5 to 3.0 eV (2.02, 2.25, 2.44 and 2.76 eV). These peaks can be compared with experimental peaks reported at 2.12, 2.28 and 2.82 eV.[6]

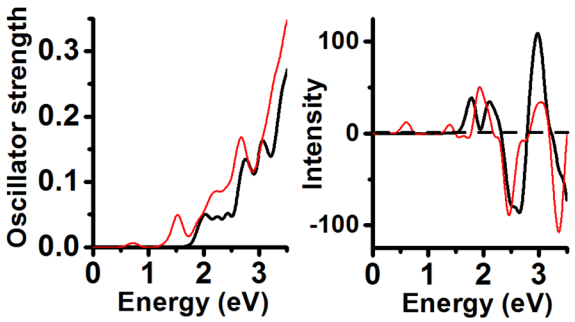

Fig. 4 Calculated UV-Vis and CD spectra of neutral $Au_{25}(SCH_3)_{19}$ clusters. PBE was used during the calculations. Black lines represent the energy minimum (Au_{11} core with a C_s symmetry, previously reported). Red lines stand for isomer with Au_{11} inner core (our C_{2v} isomer). Despite their structural differences, the calculated CD spectra show some coincidence in the range from 2.0 to 3.0 eV.

The second isomer in energy (Au_{11} and C_{2v} symmetry; 0.14 eV RE value) displayed peaks located at 0.72 eV (weak), 1.53, 1.91, 2.19 and 2.68 eV. The energy minimum shows CD peaks located at 1.77 (+), 2.11 (+), 2.65 (−), and one intense peak at 2.96 eV (+). The CD lineshape of the second energy isomer features signals located at 0.61 (+), 1.39 (+), 1.92 (+), 2.46 (−), 3.03 (+), and one intense peak located at 3.36 eV (−).

Consideration of the anionic structures yielded an increment in the energy separation among the isomers. The structure calculated with the Anionic/PBE combination has one Au_{11} core with C_{2v} symmetry, and its profile has 4 peaks included in the range from 1.5 to 3.0 eV (1.51, 1.82, 2.29 and 2.69 eV). The second isomer in energy (0.42 eV RE value) corresponding to an isomer is constituted by one Au_{11} core and C_1 symmetry. Its UV-Vis spectrum features one peak located at 0.87 eV (weak), an intense peak located at 1.55 eV and 3 more peaks under 3.0 eV (2.07, 2.36, and 2.88 eV). These 2 peaks under 2.0 eV were unexpected and not shown in the neutral/PBE case for CH_3-protected clusters (Fig. 5). This result implies that a [1−] charge state produced a large change in the calculated UV-Vis spectrum with respect to the neutral Au_{11} (C_s) cluster (Charge-state effect). Comparison of the CD spectra of both lower energy isomers of $Au_{25}(SCH_3)_{19}^{[1-]}$ clusters allows us to observe a coincidence in the position of 3 peaks included in the range from 1.0 to 2.0 eV (1.36, 1.54, and 1.88 eV). The energy minimum has one peak located at 0.50 eV (+) and a negative intense peak located at 2.65 eV. The second order in the energy isomer has one distinct negative peak located at 2.95 eV. It is noteworthy that both isomers feature weak CD profiles with respect to the neutral cases.

Anionic/TPSS combination yielded one Au_{11} isomer (C_{2v} symmetry) displaying 4 peaks in the range from 1.0 to 3.0 eV (1.5, 2.05, 2.26 and 2.69 eV). Noticeable is that 3 last peaks are close to experimental values (Fig. 6). Only the first peak located at 1.5 eV is not shown in the experimental spectrum of the neutral $Au_{25}(SR)_{19}$ cluster. The second isomer in energy comprises one Au_{14} inner core (C_1 symmetry) displaying UV-Vis peaks located at 0.82, 1.71, 2.28, and 2.54 eV. Further analysis of both CD spectra reveals that the energy minimum spectrum is less intense than the CD profile of the second isomer in energy. The energy minimum shows one negative CD peak located at 3.06 eV. The second isomer in energy (C_1) shows two intense peaks located at 1.88 eV (−) and 3.06 eV (+).

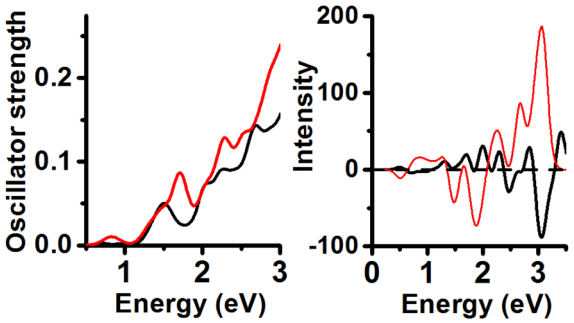

Fig. 6 Calculated UV-VIS and CD spectra of two isomers of anionic $Au_{25}(SCH_3)_{19}$ clusters. TPSS was used during optimization. Black lines represent the energy minimum (Au_{11} core with a C_{2v} point group). Red lines represent the isomer with Au_{14} inner core (C_1).

Cationic $Au_{25}(SCH_3)_{19}$ clusters were optimized using the PBE functional (Fig. 7). The energy minimum features UV-Vis peaks located at 0.84, 1.80, 2.04, 2.33, and 2.61 eV and CD peaks at 0.27 (+), 0.77 (−), 1.78 (−), 2.27 (+), and 2.63 eV (+). The second order in energy isomer has UV-Vis peaks under 1.0 eV (0.44, 0.70 eV) and 2 more peaks located at 2.03 and 2.83 eV; CD peaks at 0.36 (+), 0.91 (−), 1.27 (+), 2.04 (+), 2.50 (−) and 2.90 eV (+). It can be concluded that the effect of charge on the UV-Vis/CD spectra of isomer with inner core sustaining C_1 point group is strong.

The effect of PBE or TPSS XC-functionals (during the optimization stage) on the calculated UV-Vis or CD spectra can be summarized as follows:

(1) Neutral isomer constituted by one Au_{11} core displaying a C_{2v} symmetry optimized by either PBE or TPSS XC-functionals features similar UV-Vis and CD spectra (TDDFT calculations were carried out using the PBE XC-functional in both cases). The UV-Vis spectra depict more coincidences in peak position and in their intensity values from 0.5 to 3.0 eV (see Fig. S3†). In contrast, an isomer with one Au_{11} core (C_s symmetry) optimized

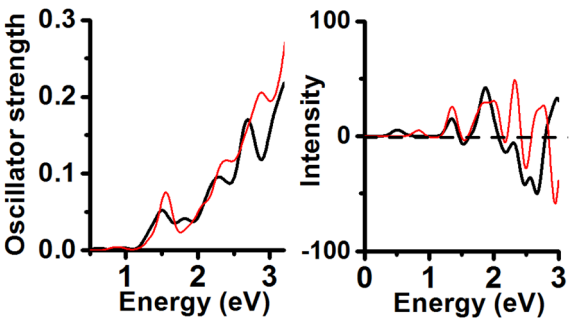

Fig. 5 Calculated UV-Vis and CD spectra of two isomers of anionic $Au_{25}(SCH_3)_{19}$ clusters. PBE was used during the calculations. Black lines represent the energy minimum (Au_{11} core with a C_{2v} symmetry). Red lines represent the isomer with Au_{11} inner core (C_1). Both UV-Vis and CD spectra feature some resemblance despite structural differences among isomers.

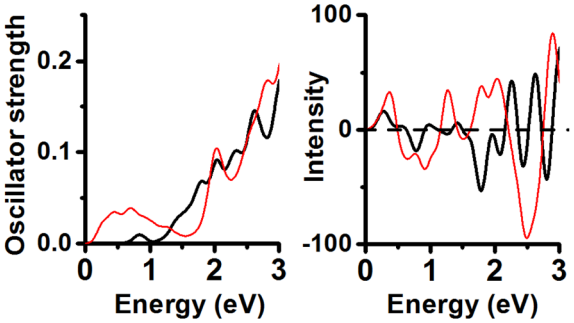

Fig. 7 Calculated UV-Vis and CD spectra of two isomers of cationic $Au_{25}(SCH_3)_{19}$ clusters. PBE was used during the calculations. Black lines represent the energy minimum (Au_{11} core with a C_{2v} point group). Red lines represent the isomer with Au_{11} inner core (C_1). Clearly, the previously reported isomer (red lines) suffers from a major shift in its UV-Vis/CD profiles.

with both XC-functionals features a pair of CD spectra with major coincidences (see Fig. S4†) rather than UV-Vis spectra.

(2) Anionic clusters with one Au_{11} core (C_{2v} symmetry) show similar UV-Vis spectra, and a further polyhedra analysis reveals 12 constituted tetrahedra (see Fig. S5†).

(3) The charge-state effect is strong in the case of isomers with inner cores of C_s symmetry, and the respective UV-Vis/CD spectra appear different (see Fig. S6†). This means that anionic structures are more distorted, resulting in fewer tetrahedra. A similar behaviour is revealed in the case of cationic structures, where structural distortion is stronger than in neutral ones, and UV-Vis/CD spectra appear more perturbed (see Fig. S7†).

(4) In the case of isomers comprising Au_{11} inner cores and sustaining a C_{2v} symmetry, neutral and anionic structures (see Fig. S8†) feature a superior match on their UV-Vis and CD profiles. Indeed, the number of constituted tetrahedra of the inner cores is preserved (12 compact tetrahedra), indicating less structural distortion with the shift of the charge state.

4 Conclusions

The provided 5-step algorithm was useful during the prediction of structures of neutral and charged $Au_{25}(SR)_{19}^{[z]}$ clusters because of its ability to predict the energy order of candidates. This algorithm was effective in determining the energetic order between the isomers of $Au_{25}(SR)_{19}^{[z]}$ clusters independently of the XC-functional/charge-state/ligand type combinations.

The new isomer constituted by one Au_{11} inner core featuring one C_{2v} symmetry is found as an energy minimum under various charge states and a combination of ligands and XC-functionals. The energy minimum of the neutral $Au_{25}(SR)_{19}$ cluster contains a pentamer motif, which is consistent with reported experimental results.[6]

The closeness in energy between our new isomer and that previously reported by Yan *et al.*[14] is remarkable. For example, in the Neutral/PBE case and by considering $-CH_3$ as ligands, a 0.14 eV RE value was obtained with respect to the isomer with one Au_{11} core (C_s symmetry).

In the case of $Au_{25}(SR)_{19}^{[1-,\ 1+]}$ clusters (R = H, CH_3), new energy minima are consistent with isomers with one Au_{11} (C_{2v}) inner core, and this result is consistent with that of the experimental data of Tandem mass spectroscopy carried out on the produced $Au_{25}(SR)_{19}^{[0]}$ cluster, revealing the presence of a lengthened motif (Au_5SR_5 unit) after ligand addition.[6]

Further analysis of isomers, including one Au_{11} inner core, allows us to know that neutral and anionic isomers feature similar UV-Vis/CD spectra for isomers with one inner core sustaining C_{2v} symmetry (Fig. S8†). This means that the charge-state effect[27,28] is minor for isomers based on a C_{2v} core.

The applicability of our 5-step algorithm is tested to find the lowest energy isomers of crystallized thiolated gold clusters, and the partial results agree with the general conclusions of this study.

Finally, it is important to mention that the search for building blocks of novel functional materials is ongoing, and several structural search methods have been proposed. This development started from naked metal clusters to ligand-protected clusters. A recent review summarizes the timeline up to artificial intelligence.[29]

Data availability

The data supporting this article have been included as part of the ESI.†

Conflicts of interest

There are no conflicts to declare.

Acknowledgements

Author acknowledges the computer resources, technical expertise and support provided by the Laboratorio Nacional de Supercómputo del Sureste de México, CONAHCyT network of National laboratories.

Notes and references

1 M. W. Heaven, A. Dass, P. S. White, K. M. Holt and R. W. Murray, *J. Am. Chem. Soc.*, 2008, **130**, 3754–3755.
2 A. Tlahuice-Flores, *Mol. Simul.*, 2012, **39**, 428–431.
3 F. P. Parker, C. A. Fields-Zinna and R. W. Murray, *Acc. Chem. Res.*, 2010, **43**, 1289–1296.
4 M. Zhu, C. M. Aikens, F. J. Hollander, G. C. Schatz and R. Jin, *J. Am. Chem. Soc.*, 2008, **130**, 5883–5885.
5 J. Akola, M. Walter, R. L. Whetten, H. Häkkinen and H. Grönbeck, *J. Am. Chem. Soc.*, 2008, **130**, 3756–3757.
6 Y. Cao, V. Fung, Q. Yao, T. Chen, S. Zang, D.-e. Jiang and J. Xie, *Nat. Commun.*, 2020, **11**, 5498–5504.
7 S. Zhuang, L. Liao, J. Yaun, N. Xiz, Y. Zhao, C. Wang and Z. Wu, *Angew. Chem., Int. Ed.*, 2019, **58**, 4510–4514.
8 M. Zhu, H. Qian, B. A. Drake and R. Jin, *Angew. Chem., Int. Ed.*, 2010, **49**, 1295–1298.
9 N. K. Chaki, H. Tsunoyama, Y. Negishi and T. Tsukuda, *J. Phys. Chem. C*, 2007, **111**, 4885–4888.
10 M. A. Muhammed, P. K. Verma, S. K. Pal, R. C. Kumar, S. Paul, R. V. Omkumar and T. Pradeep, *Chem.–A Eur. J.*, 2009, **15**, 10110–10120.
11 I. Chakraborty and T. Pradeep, *Chem. Rev.*, 2017, **12**, 8208–8271.
12 W. Xu, X. C. Zeng and Y. Gao, *Acc. Chem. Res.*, 2018, **51**, 2739–2747.
13 W. W. Xu, X. C. Zeng and Y. Gao, *Nat. Commun.*, 2016, **7**, 13574.
14 C. Yan, Y. Li, E. Wang and W. W. Xu, *J. Phys. Chem. Lett.*, 2023, **14**, 7632–7637.
15 C. B. Collins, M. A. Tofanelli, M. F. Crook, B. D. Phillips and C. J. Ackerson, *RSC Adv.*, 2017, **7**, 45061–45065.
16 M. Walter, J. Akola, O. Lopez-Acevedo, P. D. Jadzinsky, G. Calero, C. J. Ackerson, R. W. Whetten, H. Grönbeck and H. Häkkinen, *Proc. Natl. Acad. Sci. U.S.A.*, 2008, **105**, 9157–9162.

17 F. Neese, *Wiley Interdiscip. Rev.: Comput. Mol. Sci.*, 2011, **2**, 73–78.
18 P. Hohenberg and W. Kohn, *Phys. Rev.*, 1964, **136**, B864.
19 W. Kohn and L. J. Sham, *Phys. Rev.*, 1965, **140**, A1133.
20 S. Grimme, *Phys. Chem. Chem. Phys.*, 2006, **8**, 5287–5293.
21 J. P. Perdew, *et al.*, *Phys. Rev. B: Condens. Matter Mater. Phys.*, 1992, **46**, 6671.
22 (*a*) A. D. Becke, *Phys. Rev. A: At., Mol., Opt. Phys.*, 1988, **38**, 3098; (*b*) J. P. Perdew, K. Burke and M. Ernzerhof, *Phys. Rev. Lett.*, 1996, **77**, 3865.
23 J. Tao, J. P. Perdew, V. N. Staroverov and G. E. Scuseria, *Phys. Rev. Lett.*, 2003, **91**, 146401–146405.
24 M. P. Johanson, A. Lechtken, D. Schooss, M. M. Kappes and F. Furche, *Phys. Rev. A*, 2008, **77**, 053202–053209.
25 F. Mendizabal and S. Miranda-Rojas, *RSC Adv.*, 2020, **10**, 33549–33557.
26 A. Tlahuice-Flores, *J. Phys. Chem. C*, 2019, **123**, 10831–10841.
27 H. Qian, M. Y. Sfeir and R. Jin, *J. Phys. Chem. C*, 2010, **114**, 19935–19940.
28 A. Wing-Bocanegra, *Phys. Chem. Chem. Phys.*, 2019, **21**, 23855–23864.
29 J. Gao, L. Zhao, Y. Chang, Y. Zhang, S. Qiu, Y. Zhao, H. Liu and J. Zhao, *Adv. Intell. Syst.*, 2024, 2300716, DOI: **10.1002/aisy.202300716**.